THE JOURNAL OF BIOLOGICAL CHEMISTRY VOL. 291, NO. 16, pp. 8528–8540, April 15, 2016
Published in the U.S.A.

Ligand Binding Induces Conformational Changes in Human Cellular Retinol-binding Protein 1 (CRBP1) Revealed by Atomic Resolution Crystal Structures*

Received for publication, January 7, 2016, and in revised form, February 15, 2016 Published, JBC Papers in Press, February 21, 2016, DOI 10.1074/jbc.M116.714535

Josie A. Silvaroli[‡1], Jason M. Arne[‡1], Sylwia Chelstowska[‡§], Philip D. Kiser[‡¶], Surajit Banerjee[‖], and Marcin Golczak[‡ ‡‡2]**

*From the [‡]Department of Pharmacology and the [‡‡]Cleveland Center for Membrane and Structural Biology, School of Medicine, Case Western Reserve University, Cleveland, Ohio 44106, the [§]Laboratory of Hematology and Flow Cytometry, Department of Hematology, Military Institute of Medicine, Warsaw 04-141, Poland, the [¶]Research Service, Louis Stokes Cleveland Veterans Affairs Medical Center, Cleveland, Ohio 44106, the [‖]Department of Chemistry and Chemical Biology, Cornell University, Ithaca, New York 14850, and the **Northeastern Collaborative Access Team, Argonne National Laboratory, Argonne, Illinois 60439*

Important in regulating the uptake, storage, and metabolism of retinoids, cellular retinol-binding protein 1 (CRBP1) is essential for trafficking vitamin A through the cytoplasm. However, the molecular details of ligand uptake and targeted release by CRBP1 remain unclear. Here we report the first structure of CRBP1 in a ligand-free form as well as ultra-high resolution structures of this protein bound to either all-*trans*-retinol or retinylamine, the latter a therapeutic retinoid that prevents light-induced retinal degeneration. Superpositioning of human apo- and holo-CRBP1 revealed major differences within segments surrounding the entrance to the retinoid-binding site. These included α-helix II and hairpin turns between β-strands βC-βD and βE-βF as well as several side chains, such as Phe-57, Tyr-60, and Ile-77, that change their orientations to accommodate the ligand. Additionally, we mapped hydrogen bond networks inside the retinoid-binding cavity and demonstrated their significance for the ligand affinity. Analyses of the crystallographic *B*-factors indicated several regions with higher backbone mobility in the apoprotein that became more rigid upon retinoid binding. This conformational flexibility of human apo-CRBP1 facilitates interaction with the ligands, whereas the more rigid holoprotein structure protects the labile retinoid moiety during vitamin A transport. These findings suggest a mechanism of induced fit upon ligand binding by mammalian cellular retinol-binding proteins.

Effective distribution of vitamin A (all-*trans*-retinol) and its derivatives (called "retinoids") throughout the body and cellular compartments determines their essential functions in embryonic development, growth, immunology, reproduction, and vision (1–4). However, because of their lipophilic nature, free retinoids exist only at extremely low concentrations in plasma or cytosol, making diffusion kinetics between sites of action inefficient. This solubility limitation is overcome by specialized retinoid-binding proteins that regulate retinoid metabolism and physiological functions (5). Thus, an appreciation of the molecular basis for ligand uptake and targeted release by retinoid-binding proteins is critical for understanding retinoid homeostasis, yet current knowledge of this process is very limited.

Three classes of retinoid-binding proteins named for their selectivity (*i.e.* cellular retinol-binding protein (CRBP),[3] cellular retinoic acid-binding protein, and *cis*-retinoid-specific cellular retinal-binding proteins) carry vitamin A and its metabolites within cells (5–7). All representatives of CRBPs and cellular retinoic acid-binding proteins are members of intracellular lipid-binding proteins (8), whereas cellular retinal-binding protein belongs to the Sec14 protein family (9). Four CRBPs (CRBP1, -2, -3, and -4) are encoded in the human genome (10, 11). Among them, CRBP1 is the most widely expressed in numerous tissues, with the highest abundance in the liver, kidney, lung, and retinal pigment epithelium cells of the eye (12–14). In contrast, expression of CRBP2 is limited to the small intestine (15), human CRBP3 to kidney and liver (16), and CRBP4 to kidney, heart, and colon (11). CRBPs also differ in their vitamin A binding affinities. The lowest K_d values were reported for CRBP1 and CRBP2 (10–50 nM; this work) (17, 18), whereas affinity of CRBP3 and -4 for all-*trans*-retinol is lower (K_d of ~60 and 200 nM, respectively) (10, 11). These differences in expression pattern and binding affinity are consistent with the diverse physiological functions of CRBPs. In addition to serving as chaperones for the labile retinoids, accumulating evidence indicates that CRBPs are critical for the regulation of vitamin A uptake and metabolism. CRBP1 is an acceptor of retinol transported from the plasma to cytosol via a cell surface

* This work was supported by NEI, National Institutes of Health, Grant EY023948 (to M. G.) and Department of Veterans Affairs Career Development Award IK2BX002683 (to P. D. K.). The authors declare that they have no conflict of interest with the contents of this article. The content is solely the responsibility of the authors and does not necessarily represent the official views of the National Institutes of Health.

The atomic coordinates and structure factors (codes 5HBS, 5H8T, 5HA1, and 5H9A) have been deposited in the Protein Data Bank (http://wwpdb.org/).

[1] Both authors contributed equally to this work.

[2] To whom correspondence should be addressed: Dept. of Pharmacology, School of Medicine, Case Western Reserve University, 10900 Euclid Ave., Cleveland, OH 44106. Tel.: 216-368-0302; Fax: 216-368-1300; E-mail: mxg149@case.edu.

[3] The abbreviations used are: CRBP, cellular retinol-binding protein; B_{eq}, equivalent isotropic crystallographic *B*-factor; hCRBP1, human cellular retinol-binding protein 1; rCRBP1, rat cellular retinol-binding protein 1; BisTris, 2-[bis(2-hydroxyethyl)amino]-2-(hydroxymethyl)propane-1,3-diol; PDB, Protein Data Bank.

receptor named STRA6, which interacts with serum retinol-binding protein (19, 20). CRBP1 also facilitates the synthesis of retinyl esters by lecithin:retinol acyltransferase that preferentially utilizes substrate delivered by this binding protein (21). These findings are consistent with the phenotype of CRBP1-deficient mice characterized by dramatically decreased levels of retinyl esters in hepatic stellate cells and the retinal pigment epithelium. This decrease in ocular retinyl ester levels correlated with a 2-fold reduction in visual chromophore regeneration rate after light exposure due to slower diffusion of vitamin A from photoreceptors to the retinal pigment epithelium, where it is esterified (22, 23).

The ability of CRBPs to bind and transport hydrophobic compounds makes them potentially useful in delivering therapeutic agents. An example of this approach is retinylamine, an inhibitor of the visual cycle that provides protection against light-induced retinal degeneration (24, 25). The high efficacy of retinylamine is attributed to its efficient lecithin:retinol acyltransferase-driven uptake into the retinal pigment epithelium, where it exerts its therapeutic effects (26–28). Delivery of retinylamine to lecithin:retinol acyltransferase by CRBP1 can facilitate formation of retinylamides. Thus, as with vitamin A, acylation pulls retinylamine into the cells via mass action and provides a long lasting intracellular source of this drug (27, 29).

Transport of retinoids requires a precise mechanism of ligand uptake and targeted release. Despite numerous structural studies on intracellular lipid-binding proteins, neither process is yet understood. Crystal structures of mammalian fatty acid-binding protein (30, 31) and CRBP2 (32) revealed only minimal changes upon ligand binding. This is quite surprising due to the nearly completely encapsulated retinol-binding cavities in CRBP1 (33), CRBP2 (34), and CRBP3 (10) that are rather inaccessible. Thus, retinol entry and exit would require significant alterations in the positions of selected regions of the protein. This puzzle was partially resolved by NMR studies that revealed conformational flexibility at the entrance to the ligand binding pocket in apo-intracellular lipid-binding proteins (35–38). These findings led to the formulation of the "dynamic portal hypothesis" in which transient loss of structure provides a passageway for a ligand to enter an internal binding site, which would otherwise be inaccessible in the occluded conformation of the protein.

One of the main obstacles to better understanding of the role of conformational changes upon ligand binding and release by CRBPs is the lack of an apo-CRBP1 crystal structure. Therefore, to clarify this mechanistic aspect of CRBP function, we obtained the first *bona fide* x-ray structure of CRBP1 in the ligand-free form and compared it with atomic resolution structures of the protein bound to either all-*trans*-retinol or retinylamine. These analyses indicate the occurrence of well defined conformational changes involved in the binding and release of these ligands and provide evidence for conformational flexibility of the "portal" region. Thus, we provide compelling crystallographic verification of a general mechanism facilitating increased access to the binding cavity in the apo-form of mammalian CRBPs.

Experimental Procedures

Expression and purification of human Apo-CRBP1—The synthetic cDNA sequence of human CRBP1 (hCRBP1) (GI: 132387) with the addition of 6 C-terminal His residues subcloned into pD441 vector was purchased from DNA2.0. The protein was expressed in the BL21 (DE3) *Escherichia coli* strain (New England Biolabs). Bacteria were grown in a shaker incubator at 37 °C in the presence of 50 μM kanamycin. Protein expression was induced with 0.5 mM isopropyl β-D-1-thiogalactopyranoside (Roche Applied Science). After 4 h of incubation, cells were harvested by centrifugation (6,000 $\times$ *g*, 15 min, 4 °C). Bacteria were disrupted by osmotic shock (39), and the lysate was centrifuged at 36,000 $\times$ *g* for 30 min at 4 °C. Buffer composition of the supernatant was adjusted to 50 mM Tris-HCl, pH 8.0, 250 mM NaCl prior to loading onto a column filled with nickel-nitrilotriacetic acid-agarose resin (Qiagen) and equilibrated with loading buffer composed of 50 mM Tris-HCl, pH 8.0, 250 mM NaCl. The column was washed with 100 ml of loading buffer containing 5 mM imidazole, and the protein was eluted by raising the imidazole concentration to 250 mM. Fractions of the eluted protein were combined and concentrated to 5 ml in an Amicon Ultra-4 centrifugal filter with a cut-off 10,000 Da (Millipore). The protein solution then was diluted 40-fold to a final volume of 200 ml with 10 mM Tris-HCl buffer, pH 8.0, and loaded onto a Mono-Q ion exchanger column (GE Healthcare). hCRBP1 was eluted with a gradient of NaCl (0–0.5 M) over 30 min at a flow rate 0.5 ml/min. Collected fractions were examined by SDS-PAGE, and those containing purified hCRBP1 were pooled together (Fig. 1*A*). The protein was concentrated to 3 mg/ml, and 0.2-ml aliquots were stored at −80 °C.

Synthesis of All-trans-retinylamine—All-*trans*-retinylamine (retinylamine) was synthesized by reacting 0.5 g of all-*trans*-retinal (Toronto Research Co.) dissolved in 5 ml of ethanol with ammonia (7 N in methanol (Sigma-Aldrich)) (24). After 2 h of stirring at room temperature, the resulting retinyl imine was reduced by sodium borohydride (Sigma-Aldrich). To avoid formation of side products and increase product yield, retinyl imine solution was added dropwise to 200 ml of ethanol containing a stoichiometric excess of sodium borohydride. The reduction reaction was carried out for 2 h on ice with vigorous stirring. Retinoids were extracted with ethyl acetate, and the organic solvent was washed twice with a saturated solution of NaCl and loaded onto a silica gel (Sigma-Aldrich). After an extensive wash with ethyl acetate, retinylamine was eluted with a mixture of methanol, ethyl acetate, and 7 N ammonia in methanol (49.5:50:0.5, v/v/v, respectively). The purity of retinylamine was verified by HPLC using a normal phase Luna 10-μm PREP silica 100-Å, 250 $\times$ 4.6-mm column (Phenomenex) and ethyl acetate with 0.5% ammonia solution as the mobile phase at a flow rate of 2.0 ml/min.

Retinoid Fluorescence Binding Assays—The affinity of all-*trans*-retinol or retinylamine for hCRBP-I was evaluated by monitoring the quenching of protein fluorescence at increasing concentrations of the ligand. All measurements were performed on a PerkinElmer Life Sciences LS55 model fluorometer. After the excitation wavelength was set at 285 nm, emission

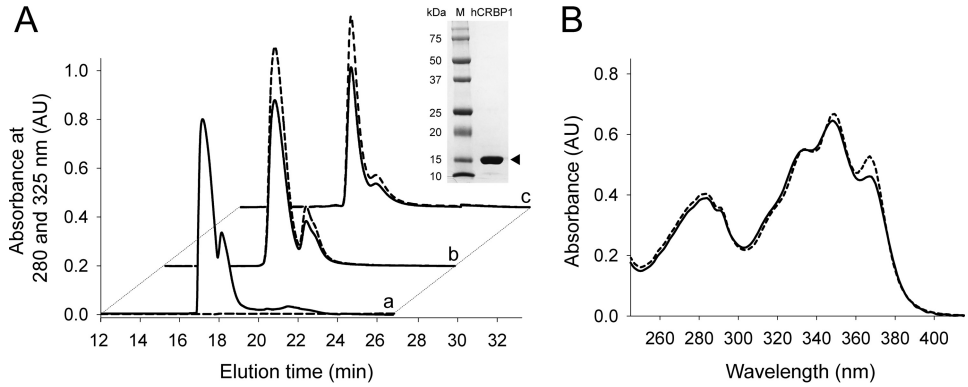

FIGURE 1. **Purification of recombinant hCRBP1 and formation of complexes with all-*trans*-retinol and retinylamine.** *A*, elution profile of apo- (*a*), all-*trans*-retinol- (*b*), and retinylamine-bound (*c*) proteins from a Mono-Q ion exchanger column. *Solid* and *dashed traces*, absorbance at 280 and 325 nm, respectively. *Inset*, SDS-PAGE of purified hCRBP1 after Coomassie Blue R-250 staining. *Arrowhead*, position of expressed protein in a 12% polyacrylamide gel. *B*, absorbance spectra of hCRBP1 in complex with all-*trans*-retinol (*solid line*) and retinylamine (*dashed line*) collected in 10 mM Tris-HCl buffer, pH 8.0. *AU*, absorbance units.

spectra were recorded between 300 and 420 nm with bandwidths for excitation and emission fixed at 10 nm. Titrations were carried out at 25 °C in 20 mM Tris-HCl buffer, pH 7.6, containing 50 mm NaCl and 5% glycerol (v/v). Concentrations of all-*trans*-retinol and retinylamine stock solutions were determined spectrophotometrically by using the molar absorbance coefficient $\epsilon = 52{,}770$ for the maximum absorbance at 325 nm in ethanol (40). Retinoids were delivered in DMSO. Final concentrations of the solvent did not exceed 0.2% of the sample's total volume. All binding data were corrected for background and self-absorption of excitation and emission light (41). Apparent K_d values were calculated by nonlinear regression of the experimental data using saturation ligand-binding models available in the SigmaPlot software package (Systat Software).

Formation of Holo-hCRBP1 with All-trans-retinol or Retinylamine—To obtain holo-hCRBP1, 3 mg of the apoprotein was incubated for 20 min on ice in 10 mM Tris-HCl, pH 8.0, 10% glycerol (v/v) with either all-*trans*-retinol (Toronto Research Company) or retinylamine delivered in DMSO (2%, v/v) to a final concentration of ~0.2 mM (~2-fold molar excess over the protein). To remove unbound retinoids, the protein solution was diluted 10-fold with 10 mM Tris-HCl, pH 8.0, and centrifuged to remove potential precipitates (36,000 × *g*, 20 min, 4 °C). Holo-hCRBP1 was repurified on a Mono-Q column as described above. The effectiveness of holo-hCRBP1 formation was verified spectrophotometrically. The complex of hCRBP1 with all-*trans*-retinol or retinylamine revealed an A_{350}/A_{280} ratio of 1.6, as reported previously for holo-CRBP1 purified from rat liver (Fig. 1*B*) (42).

Crystallization Conditions—hCRBP1 in complex with all-*trans*-retinol or retinylamine as well as the apoprotein was crystallized with the sitting drop vapor diffusion method. Protein samples at 3 mg/ml concentration were mixed in a 1:1 ratio with 1.3 μl of 0.1 M BisTris, pH 5.5, and 25% PEG 6000 or PEG 3350. Plates were sealed and incubated at room temperature. Rodlike crystals with dimensions of 0.2–1.0 mm in length and 10–25 μm in width grew within 2–5 days. Mature crystals were collected and flash-cooled in liquid nitrogen in preparation for x-ray diffraction experiments.

Verification of Complex Stability between hCRBP1 and Retinylamine—Fifty μg of the protein was extracted with ethyl acetate. The organic phase was collected, and the solvent was dried down in a stream of nitrogen. Retinoids were resolubilized in 100 μl of acetonitrile; loaded onto a reverse phase Gemini 5-μm, 100-Å, 250 × 4.6-mm C18 column (Phenomenex); and eluted with a gradient of 20–100% acetonitrile in water developed over 20 min at a flow rate of 1.5 ml/min. Both solvents contained 0.1% (v/v) formic acid. Similar analyses were performed using retinylamine holo-hCRBP1 crystals. Ten protein crystals were harvested and washed three times by transferring them to fresh crystallization solutions. Finally, the resulting crystals were dissolved in 50 μl of 50% methanol/water (v/v), and retinoids were extracted with ethyl acetate and analyzed by HPLC as described above.

X-ray Data Collection—Diffraction data for apo-hCRBP-I crystals (PDB code 5H9A) and all-*trans*-retinol holo-hCRBP1 crystals (PDB code 5H8T) were collected at NE-CAT beamline 24-ID-C at the Advanced Photon Source at Argonne National Laboratory. Data were collected in the shutterless mode by a Dectris Pilatus 6MF pixel array detector with 0.5° images at 0.9792-Å wavelength and a 300-mm crystal-to-detector distance. Data for the hCRBP1 complex with retinylamine (PDB code 5HA1) were obtained at NE-CAT beamline 24-ID-E with an ADSC Quantum 315 CCD detector at the Advanced Photon Source at Argonne National Laboratory. The detector distance was 150 mm, oscillation range was 1.0°, and wavelength was 0.9792 Å. An ultra-high resolution data set for all-*trans*-retinol holo-hCRBP1 (PDB code 5HBS) was collected at the BL12-2 beamline at the Stanford Synchrotron Radiation Lightsource equipped with a Pilatus 6M PAD detector. Images were measured at 0.2° increments by using an x-ray wavelength of 0.7293 Å at a 200-mm crystal-to-detector distance.

Data Processing, Model Building, and Refinement—Data from single crystals of apo- and holo-hCRBP1 were integrated and scaled with Mosflm (43). The 0.89 Å resolution data set for hCRBP1 bound to all-*trans*-retinol was processed with XDS (44). The structure of hCRBP1 was solved by molecular replacement with PHASER_MR (45) using the atomic coordinates of rat CRBP1 (rCRBP1) in complex with all-*trans*-retinol (PDB

TABLE 1
X-ray data collection and refinement statistics

	CRBP1 (all-*trans*-retinol)	CRBP1 (all-*trans*-retinol)	CRBP1 (retinylamine)	CRBP1 (APO)
PDB accession code	5HBS	5H8T	5HA1	5H9A
Beam line	BL12-2	24-ID-C	24-ID-E	24-ID-C
Wavelength (Å)	0.7293	0.9792	0.9792	0.9792
Data collection				
Space group	$P2_12_12_1$	$P2_12_12_1$	$P2_12_12_1$	$P2_12_12_1$
Cell dimensions				
a, *b*, *c* (Å)	37.22, 49.77, 73.48	37.50, 44.99, 84.97	37.15, 49.57, 73.30	37.35, 37.96, 94.96
α, β, γ (degrees)	90, 90, 90	90, 90, 90	90, 90, 90	90, 90, 90
Resolution (Å)	33.20–0.89 (0.94–0.89)[a,b]	37.55–1.21 (1.23–1.21)[a]	27.55–1.35 (1.32–1.35)[a]	47.48–1.38 (1.41–1.38)[a]
R_{sym} (%)	8.8 (89.7)	7.4 (50.4)	10.3 (60.4)	8.2 (59.9)
$I/\sigma I$	24.5 (3.2)	10.6 (1.9)	9.4 (3.2)	11.0 (2.8)
Completeness (%)	98.7 (92.7)	99.4 (98.5)	100 (100)	98.9 (98.9)
Redundancy	12.4 (10.4)	5.0 (4.2)	5.9 (5.9)	5.3 (4.6)
Refinement				
Resolution (Å)	33.20–0.89	34.35–1.21	27.55–1.35	35.25–1.38
No. of reflections	104,073	44,760	30,442	28,067
R_{work}/R_{free} (%)	12.5/13.3	11.8/14.7	12.2/15.6	13.3/17.1
No. of atoms	1580	1529	1502	1362
Protein	1223	1198	1196	1180
Ligand	21 (RTL)[c]	21 (RTL)[c]	21 (RNE)[c]	14 (BTB)[c]
Water	336	310	285	168
Mean *B*-factor (Å^2)				
Protein	6.2	9.6	8.3	18.8
Ligand	6.9 (RTL)[c]	10.1 (RTL)[c]	15.1 (RNE)[c]	20.5 (BTB)[c]
Water	14.9	25.5	17.2	30.5
Root mean square deviations				
Bond lengths (Å)	0.005	0.009	0.010	0.011
Bond angles (degrees)	0.989	1.194	1.131	1.123
Validation				
Ramachandran plot				
Favored/outliers (%)	98.0/0[d]	97.9/0[d]	98.6/0[d]	99.3/0[d]

[a] Reported data set was collected on a single crystal.
[b] Values shown in parentheses are for the highest resolution shell.
[c] Ligand accession code.
[d] As defined by MolProbity.

code 1CRB). Models were built and manually adjusted in COOT (46, 47), including adding alternative conformations where appropriate and refined with PHENIX (48), using a riding hydrogen model, individual anisotropic temperature factors, and occupancy refinement for alternative conformers and waters. Allowing individual hydrogen refinement did not result in better geometry statistics or R factors. Geometry of the refined models was assessed with the MolProbity server (49). The final atomic coordinates and structure factors for all four structures described in this paper were deposited in the RCSB Protein Data Bank. The accession codes as well as the data collection and refinement statistics are summarized in Table 1. Visualization of the macromolecules and figure preparation were carried out with the CHIMERA software package version 1.10.1 (50).

Calculations of Average Crystallographic B-Factors and Distribution of Anisotropy within Refined Models—To compare residue mobility, the averages of the equivalent isotropic crystallographic *B*-factors (B_{eq}) for the main chain of each residue were calculated. They represent isotropic displacement of atoms that were described by anisotropic displacement parameters during refinement. Then the residue B_{eq} values were normalized with the "*z*-score normalization" methodology (51),

$$B_{eqX-zscore(i)} = [B_{eqX(i)} - \langle B_{eq}\rangle_{(i)}]/S_{(i)} \quad \text{(Eq. 1)}$$

where $B_{eqX\text{-}zscore(i)}$ is the normalized *z*-score for residue *X* in structure i, $B_{eqX(i)}$ is the equivalent isotropic *B*-factors for residue *X*, $\langle B_{eq}\rangle_{(i)}$ is the average residue equivalent isotropic *B*-factor for structure i, and $S_{(i)}$ is the corresponding standard deviation among atoms in the structure.

The anisotropy of individual atoms, defined as the ratio of the minimum and maximum eigenvectors of the anisotropic displacement parameter matrix (52), as well as the anisotropy mean values for the protein structures were calculated using PARVATI (53) and ANISOANL (47) validation tools.

Results

High Resolution Structure of hCRBP1 in the Retinol-bound State—Nearly all crystallographic information about CRBPs originates from structures of CRBP2. CRBP1 is represented by only a single set of crystallographic coordinates for a holoprotein purified from rat liver refined at a modest resolution of 2.1 Å (PDB code 1CRB) (33). Attempts to replicate the previously reported rCRBP1 crystallization conditions, which included cadmium (II) chloride as a precipitant (54), were unsuccessful in the case of hCRBP1. Crystals instead were obtained from PEG 6000- or PEG 3350-containing solutions. Despite the differing crystallization conditions, hCRBP1 crystals grew in space group $P2_12_12_1$ with unit cell constants similar to those of rCRBP1 with a single protein molecule in the asymmetric unit.

The 0.89 and 1.21 Å structures of hCRBP1 (PDB codes 5HBS and 5H8T, respectively) reported here represent a significant improvement over rCRBP1 reported previously (33). Their higher resolution facilitated the building of a more accurate model of the structure, including residues directly involved in retinoid binding. In fact, the electron density maps are well

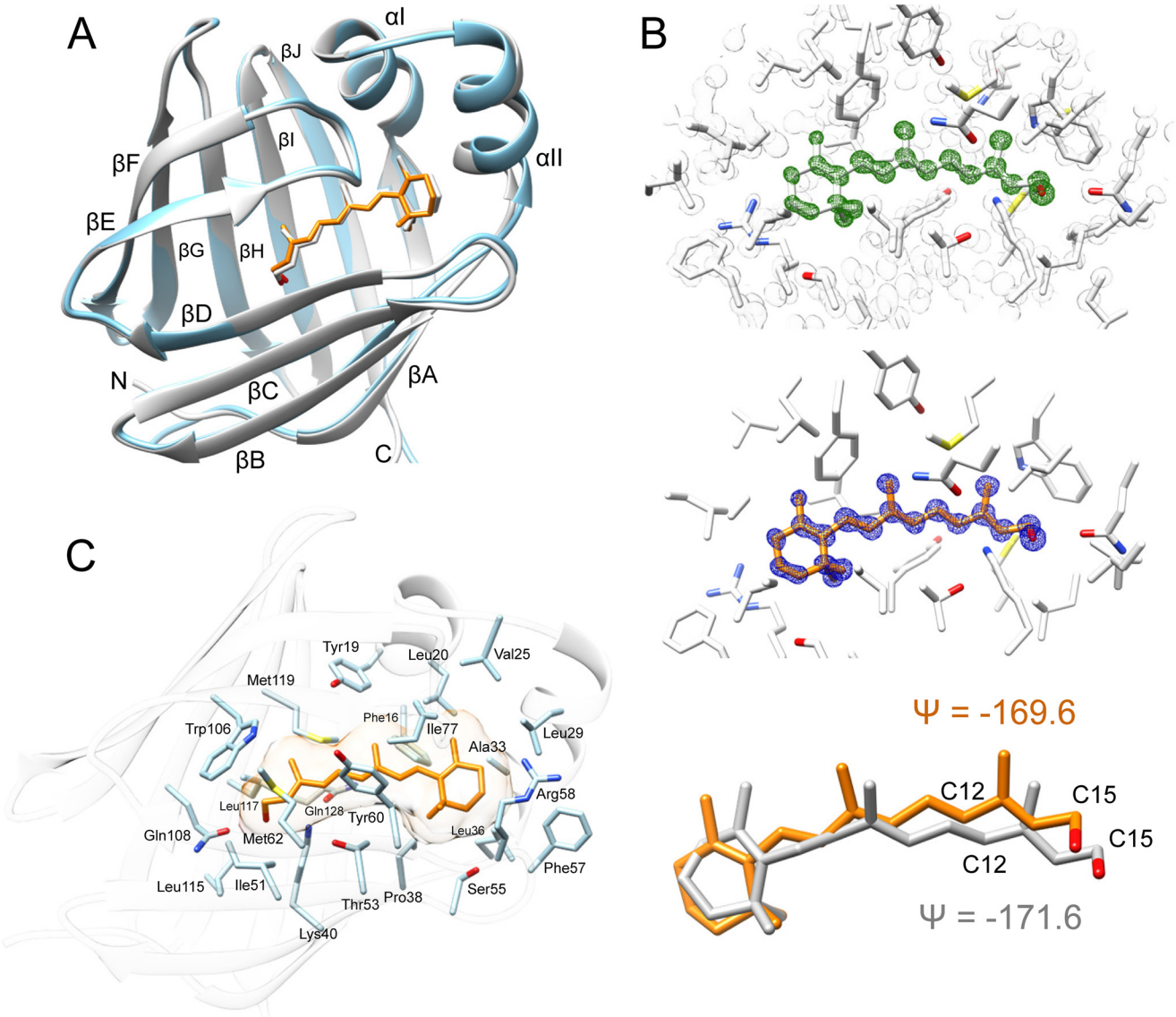

FIGURE 2. **Crystal structure of all-*trans*-retinol holo-hCRBP1.** *A*, *ribbon diagrams* of overlay structures of hCRBP1 depicted in a *light blue color* (PDB code 5HBS) and rCRBP1 *colored* in *gray* (PDB code 1CRB). *B*, electron density maps for all-*trans*-retinol and the ligand geometry. In the *top panel*, the *green mesh* represents an unbiased 0.89 Å resolution σA-weighted $F_o - F_c$ omit electron density map contoured at 6.0σ. The appearance of a strong positive electron density clearly indicates the location of the retinoid moiety. The *gray mesh* corresponds to the $2F_o - F_c$ electron density map contoured at 2.0σ. The *middle panel* signifies a refined $2F_o - F_c$ electron density map for the ligand at 1.6σ shown in *blue*. The *bottom panel* shows torsion angles between carbons C12-C13/C14-C15 of the retinoid moiety found in the x-ray structures of hCRBP1 (*orange*) and human CRBP2 (*gray*), PDB code 5HBS and 4QZT, respectively. *C*, molecular organization of the retinoid-binding pocket with selected residues proposed to be involved in formation of the internal cavity.

defined for all of the residues, including the C-terminal histidine residues of a His_6 tag, with the exception of the Lys-68 side chain. The overall structure of hCRBP1 closely resembles those of other intracellular lipid-binding proteins with a compact single-domain architecture composed of 10 β-strands organized in two anti-parallel β-sheets (Fig. 2*A*). These form a flattened β-barrel that surrounds the retinoid-binding site. One of the two potential entrances to this site is completely enclosed by the side chains of the β-sheets and the N terminus, whereas the other is protected by two short α-helices (I and II) and the hairpin turns between β-strands βC-βD and βE-βF. These α-helices and turns constitute a so-called "portal region." Holo-hCRBP1 and holo-rCRBP1 exhibit high structural similarity with an overall root mean square deviation of 0.89 Å between equivalent main chain atoms (Table 2).

Electron density for all-*trans*-retinol was well defined for the entire molecule, thereby allowing all of the ligand atoms to be refined at 100% occupancy. The retinoid moiety is almost planar. The β-ionone ring is embedded in a hydrophobic cleft between α-helices I and II, and it turns connecting β-strands βC-βD and βE-βF. The orientation of the β-ionone ring is essentially identical to those found in other CRBPs and adopts the 6-*s*-*trans* configuration (Fig. 2*B*). The dihedral angles defined by atoms C5-C6/C7-C8 in PDB entries 5HBS and 5H8T are nearly identical, with $\psi = -152.3$ and $-153.9°$, respectively. Free rotation of the β-ionone ring is restricted by hydrophobic side chains of Phe-16, Phe-57, Leu-36, Val-25, Leu-29, and Leu-20 (Fig. 2*C*). The first residue seems to be particularly important for defining the ring position. An alternative 6-*s*-*cis* configuration would cause steric clashes between the *gem*-dim-

TABLE 2

Root mean square deviations between various holo- and apo-forms of CRBP1

Root mean square deviation values were calculated for the main chain atoms of entire polypeptide chains (normal type) and the portal regions (residues 24–36, 53–60, and 73–81) (italic type) of available CRBP1 structures. Root mean square deviation values for apo- *versus* holo-pairs are shown in boldface type. All values were calculated using Baverage software available in the CCP4 package (45).

	Root mean square deviation				
	Holo (retinol), 0.89 Å, PDB code 5HBS	Holo (retinol) 1.21 Å, PDB code 5H8T	Holo (retinylamine), PDB code 5HA1	Apo, PDB code 5H9A	Rat holo (retinol), PDB code 1CRB
			Å		
Holo (retinol), 0.89 Å, PDB code 5HBS		*0.42*	*0.15*	***1.84***	*0.83*
Holo (retinol) 1.21 Å, PDB code 5H8T	0.38		*0.33*	***1.71***	*0.70*
Holo (retinylamine), PDB code 5HA1	0.27	0.29		***1.76***	*0.77*
Apo, PDB code 5H9A	**1.07**	**0.92**	**0.97**		*1.79*
Rat holo (retinol), PDB code 1CRB	0.89	0.65	0.83	**1.08**	

ethyls and the Phe-16 side chain benzyl ring (Fig. 2*C*). The rest of the ligand binding cavity is lined with well conserved hydrophobic residues that provide non-polar interactions with the retinoid moiety.

Several structures of CRBP2 and CRBP from zebrafish contained degradation products of the labile retinoid moiety caused by x-ray radiation exposure (34, 55, 56). These were characterized by the alteration of torsion angles measured between carbons C12-C13/C14-C15 along the polyene chain that were not consistent with the geometry of a *trans* double bond. This aberration caused spatial relocation of the hydroxyl group and formation of hydrogen bonds with the side chain of Lys-40 in addition to the canonical Gln-108. We found no evidence for radiation damage of all-*trans*-retinol in the hCRBP1 structures. The torsion angles for C12-C13/C14-C15 were $\psi = -169.6$ and $-169.1°$ in the 0.89 and 1.21 Å structures, respectively. These values are nearly identical to those found in retinol bound to human CRBP2 (PDB code 4QZT), a model structure for which crystallographic data were collected at low x-ray energy (34) (Fig. 2*B*). Interestingly, optimal geometry of all-*trans*-retinol in hCRBP1 does not prevent the hydroxyl group from hydrogen-bonding with side chains of both Gln-108 and Lys-40 (Fig. 3*A*). This finding represents a major dissimilarity between previous models of rCRBP1 or CRBP2 and current high resolution hCRBP1 structures. The key difference that permits direct formation of a hydrogen bond with Lys-40 is the position of its side chain, which adopts a conformation distinct from those previously reported by bringing the ζ-nitrogen atom ~1.0 Å closer to the hydroxyl group of vitamin A (Fig. 3*A*). Importantly, the electron density for the entire Lys-40, including every atom of the side chain, is very well defined, and the geometric parameters for this residue are well within allowed ranges. Also, there is no difference in the position of Lys-40 between the 0.89 and 1.21 Å data sets. The side chain conformation of Lys-40 is stabilized by a network of hydrogen bonds between the hydroxyl group of Thr-53 and the water molecule, Wat-1 (*W1* in Fig. 3*B*). Wat-1 further interacts with ϵ^1-carbonyl oxygen of Gln-128 and with water Wat-2, which in turn is hydrogen-bonded to the ϵ^2-amino group of Gln-128. Additionally, Thr-53 interacts with Wat-3 to complete the functional network of the hydrogen bonds. The high-resolution structure reveals a total of seven well defined water molecules buried in the binding site, all of which interact with internal polar side chains. Waters Wat-4, -5, and -6 form yet another network, in which Wat-4 interacts with the ϵ^1-nitrogen atom of the Trp-106 indole ring, Wat-6 interacts with the hydroxyl group of Tyr-19, and Wat-5 bridges these two water molecules together. Finally, Wat-7 interacts with side chains of Tyr-19 and Gln-97.

hCRBP1 in Retinylamine-bound State—To shed light on the role of hydrogen bonds within the retinoid-binding pocket, we co-crystallized hCRBP1 with retinylamine, a retinol derivative in which a hydroxyl is replaced by an amino group. Prior to crystallization, we verified that labile retinylamine was stable in its hCRBP1-bound state by determining the composition and quantity of retinoids extracted from retinylamine holo-hCRBP1 after 2 days of incubation at room temperature. As shown in Fig. 4*A*, an HPLC chromatogram revealed a single retinoid peak, with an elution time and a UV-visible absorbance spectrum that perfectly matched that of a synthetic retinylamine standard. The amount of extracted retinylamine and number of the protein molecules were closely correlated, revealing ~1.1 stoichiometry. The same analyses performed on retinylamine holo-hCRBP1 crystals indicated the presence of retinylamine in the crystalline form of the protein.

Comparison of the aligned structures of hCRBP1 in complex with all-*trans*-retinol and retinylamine indicated a similar positioning of the two ligands within the binding pocket (Fig. 4*B*). Thus, the amino group of retinylamine is perfectly located to form a hydrogen bond with ϵ^1-carbonyl oxygen of Gln-108. In contrast, an interaction between protonated amino groups of the ligand (pK_a ~7.2) (27) and Lys-40 would be unfavorable due to electrostatic repulsion. Thus, only a single hydrogen bond could be made to stabilize retinylamine binding. To investigate whether the alteration of the hydrogen bonding affects ligand binding, we determined the dissociation constant for all-*trans*-retinol and retinylamine with a fluorescence quenching assay. As shown in Fig. 4*C*, incubation of these retinoids with hCRBP1 led to an exponential decay of protein fluorescence that displayed a saturable binding isotherm. Subsequent calculation of the apparent dissociation constants revealed a $K_d = 18.5 \pm 1.1$ nM for all-*trans*-retinol and a $K_d = 64.1 \pm 16.9$ nM for retinylamine. This result identifies the ability of hCRBP to form hydrogen bonds with side chains of both Lys-40 and Gln-108 as a major factor responsible for its nearly 4 times higher affinity for all-*trans*-retinol than retinylamine.

Comparison of Apo- and Holo-structures of hCRBP1—The enclosed retinoid-binding cavity observed for holo-hCRBP1 raises the question of whether the apoprotein structure would reveal any conformational differences that could allow ligand binding. Comparison of both all-*trans*-retinol- and retinyl-

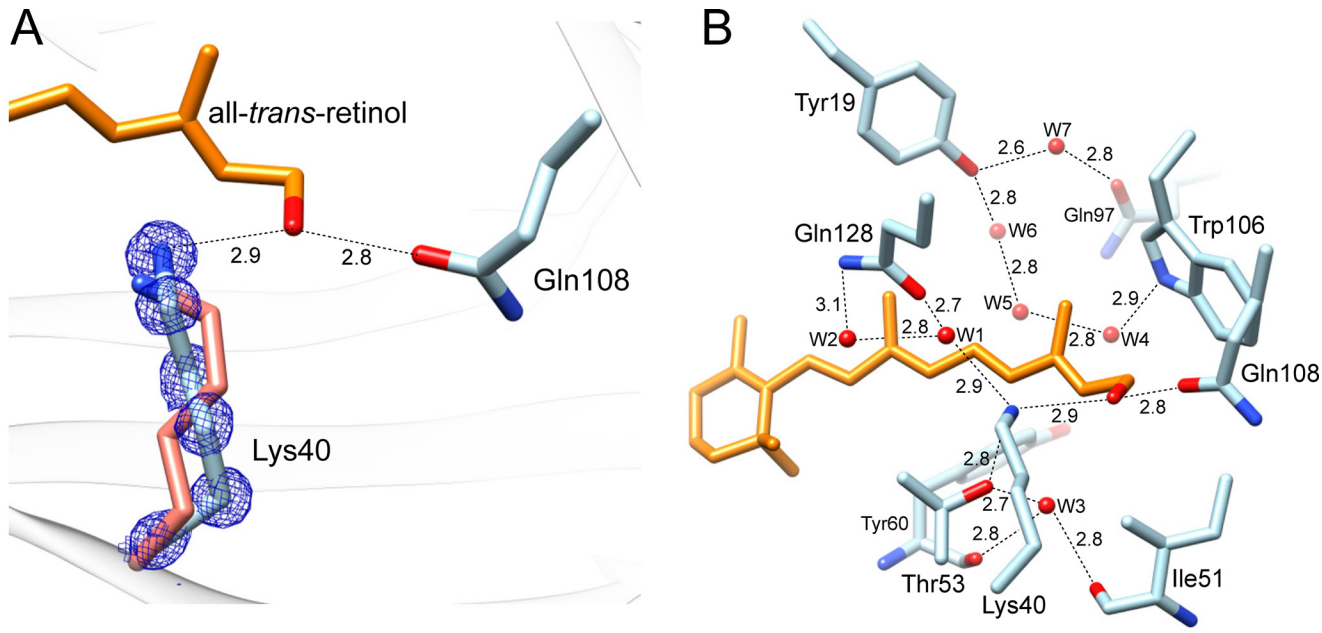

FIGURE 3. **Interaction of the hydroxyl group of vitamin A in the binding pocket.** *A*, orientation of the side chains and local interactions of Lys-40 and Gln-108. The side chain of Lys-40 in rCRBP1 is shown in *salmon color*, whereas the side chains of the human protein are *tinted* in *light blue*. *Blue mesh*, $2F_o - F_c$ electron density map for the side chain of Lys-40 in hCRBP1 contoured at 2.0σ. Hydrogen bonds are indicated by *dashed lines*. Distances are shown in Å. *B*, hydrogen bond network in the retinoid-binding pocket of hCRBP1. Water molecules (*W*) are shown as *red spheres*.

amine-bound structures with the ligand-free model revealed a high level of conservation of the overall structure. The root mean square deviation values calculated for the main chain atoms of superimposed holo- and apo-structures ranged between 0.92 and 1.07 Å (Table 2). However, they are significantly larger (1.7–1.8 Å) in discrete regions, including α-helix II (residues 24–36) as well as the hairpin βE-βF and βC-βD turns (residues 53–60 and 73–81, respectively) (Fig. 5, *A* and *B*). These differences reflect conformational rearrangements of hCRBP1 in the absence of a ligand. The most significant transition is repositioning of the main chains of βC-βD and particularly the βE-βF loops toward the interior of the retinoid-binding cavity, accompanied by α-helix II bending away from the rest of the protein.

Rearrangement of the main chains is followed by displacement of the side chains of several residues that surround vitamin A. The most striking changes are noted for Phe-57, Tyr-60, Leu-74, and Ile-77 (Fig. 5*C*). Their side chains adopt orientations that protrude into the binding cavity, occupying space reserved for the β-ionone ring of retinoid in the holo-structures. Concomitantly, the side chains of Phe-16, Leu-20, Val-25, and Leu-29 that belong to α-helix II are pushed backward to avoid close contact with Phe-57 and Ile-77. Interestingly, the remaining amino acids that line the interior of the binding pocket do not change their orientations upon the holo to apo transition. This observation could be explained by a preserved hydrogen-bonding network in which a hydroxyl group of retinol is substituted by a water molecule in the apo-structure, underscoring the important structural role of waters in hCRBP1 (Fig. 5*D*).

Backbone Dynamics of Apo- and Holo-hCRBP1—The conformational changes described above seem counterintuitive because they provide evidence for a significant steric hindrance that prevents entrance of vitamin A into the apoprotein's binding pocket. Although crystals of apo- and holo-hCRBP1 are not isomorphous, dissimilarities in the crystallographic intermolecular contacts do not affect the protein regions that reveal conformational changes. Thus, the differences observed can be attributed to the presence or absence of a ligand rather than crystal packing. In an attempt to explain this phenomenon, we closely examined the atomic positions in the refined models. Contrary to the structures of holo-hCRBP1, where the electron density was very well defined throughout the model, we found only satisfactory electron densities for the main chain and poor electron densities for part of the side chain in the portal region of apoprotein (Fig. 6). This observation suggests that some regions of the apo-hCRBP1 could exhibit significantly greater conformational flexibility. To further evaluate the dynamics of the portal region in a more quantitative manner, we analyzed the equivalent isotropic crystallographic *B*-factors (B_{eq}). Because B_{eq} values could be affected by refinement strategies or differences in data resolution, they were scaled by the *z*-score normalization method (51) before the analysis. To further ensure proper interpretation of any differences, we compared B_{eq} values for the main chain atoms of the apoprotein with both the 0.89 and 1.21 Å structures of all-*trans*-retinol-bound hCRBP1 as well as with its retinylamine-bound form. Also, as an internal control, we calculated the corresponding differences between all-*trans*-retinol and retinylamine holoproteins. All comparisons of the normalized crystallographic *B*-factors between apo- and holo-forms of hCRBP1 were very consistent with each other, leading to the conclusion that the higher backbone mobility occurs at the well defined portal region of the protein (Fig. 6). Importantly, these differences were not seen among the holo-structures. Thus, the ligand-free crystal structure most likely represents a dominant conformation (but only one of many possible conformations) of the apoprotein.

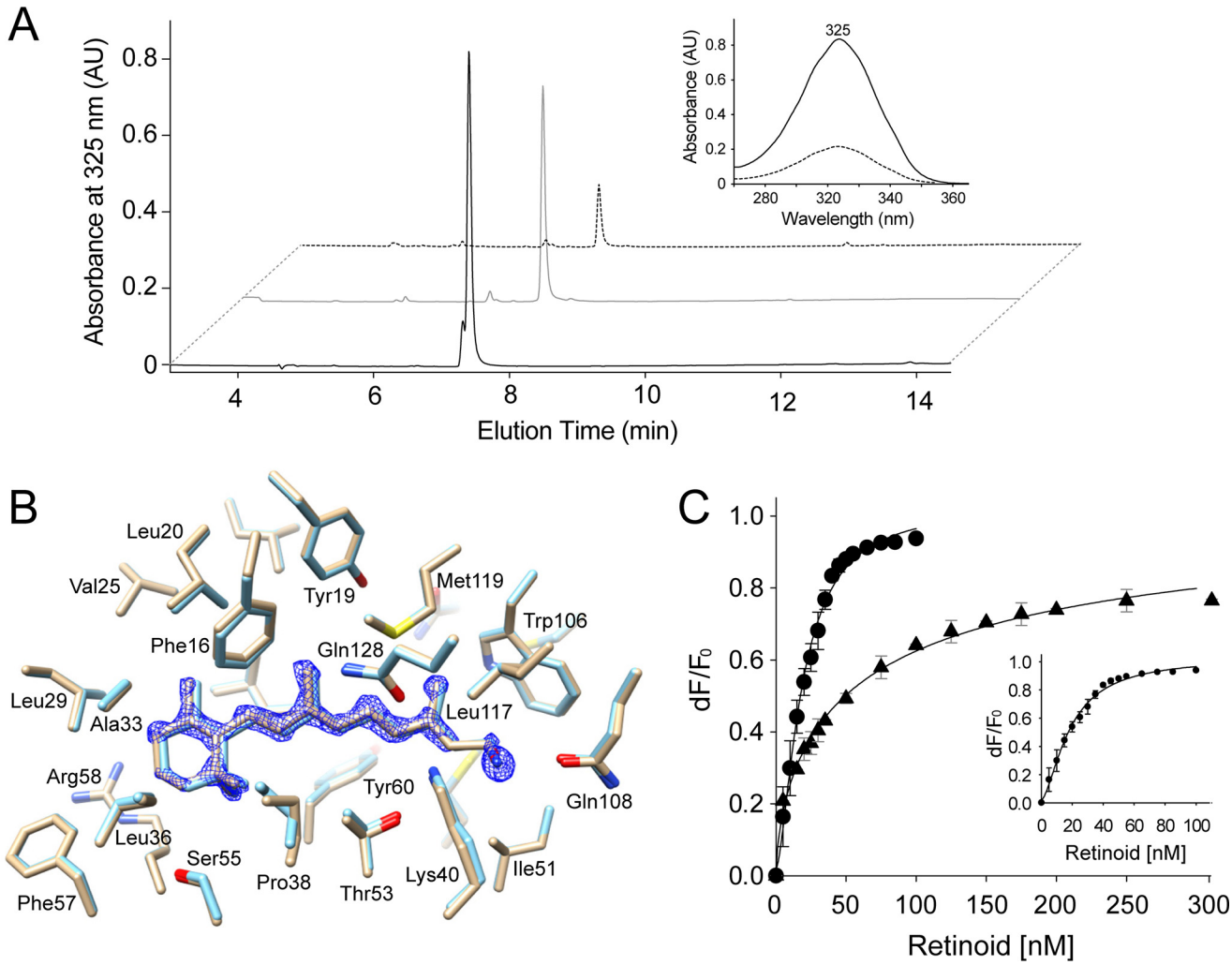

FIGURE 4. **Binding of retinylamine to hCRBP1.** *A*, to determine the retinoid composition carried by hCRBP1 preincubated with retinylamine, the protein was extracted with ethyl acetate, and the retinoids were analyzed by reverse phase HPLC. The chromatograms revealed a single peak (*black trace*) with an elution time and UV-visible absorbance spectrum (*inset*) that perfectly match that of a synthetic retinylamine standard (*gray trace*). Similar analyses performed on the protein crystals also revealed a robust peak corresponding to retinylamine (*dashed trace*). *B*, an overlay of the side chains at the binding site of hCRBP1 in complex with all-*trans*-retinol (*light blue*, PDB code 5HBS) and retinylamine (*light orange*, PDB code 5HA1). The *blue mesh* represents a $2F_o - F_c$ electron density map for retinylamine contoured at 1.6σ. *C*, determination of the apparent dissociation constants for all-*trans*-retinol and retinylamine. Quenching of the maximum fluorescence emissions upon increasing concentrations of all-*trans*-retinol (●) or retinylamine (▲) were monitored at 337 nm, corrected for background and inner filter effects, and used to calculate the apparent K_d values, which are 18.5 ± 1.1 nM for all-*trans*-retinol and 64.1 ± 16.9 nM for retinylamine. The *inset* represents an expanded titration curve for all-*trans*-retinol. All experiments were repeated three times in duplicate. Data are presented as mean values ± S.D. *AU*, absorbance units.

In addition to the magnitude of atomic displacement, experimental anisotropic *B*-factors provide information about preferred directions of atomic movement. As analyzed by the PARVATI software, the mean anisotropy for all non-hydrogen protein atoms in hCRBP1 structures are as follows: 0.37 (σ 0.11) for apo-, 0.35 (σ 0.10) for all-*trans*-retinol holo-, and 0.40 (σ 0.12) for retinylamine-bound proteins. Slightly lower anisotropy, 0.54 (σ 0.13), is observed for 0.89 Å holo-hCRBP1, which correlates with exceptionally low thermal *B*-factors for this structure. Nevertheless, these values deviate significantly from 1, which represents perfect isotropy. Contrary to the B_{eq}, the anisotropy parameters revealed low variability along the polypeptide chains and were not affected by the ligand binding. Although analysis of the Rosenfield plots (57) indicated that the quasi-rigid body model cannot be applied to the parts of hCRBP1 that form the portal region, it is interesting to note significant changes in the directional preference of individual atom fluctuations in the turn connecting β-strands βE-βF (Fig. 7). In addition to an increase in the level of motion, movement of the main chain atoms in apo-hCRBP1 is characterized by the major vibrational axes oriented toward and being almost parallel to the anisotropy axes of loop βC-βD. This dynamic flexibility in combination with positions of the side chains of Phe-57, Arg-58, Tyr-60, and Ile-77, can further contribute to narrowing the aperture of the portal. Binding of vitamin A greatly affects the conformation of the βE-βF turn and induces a change in the orientation of the major vibrational axes. They become nearly perpendicular to that observed in the apo-structure and are directed toward the retinoid molecule.

Overall, the above data provide evidence that binding of all-*trans*-retinol or retinylamine increases local backbone stability, locking hCRBP1 in a well defined conformation.

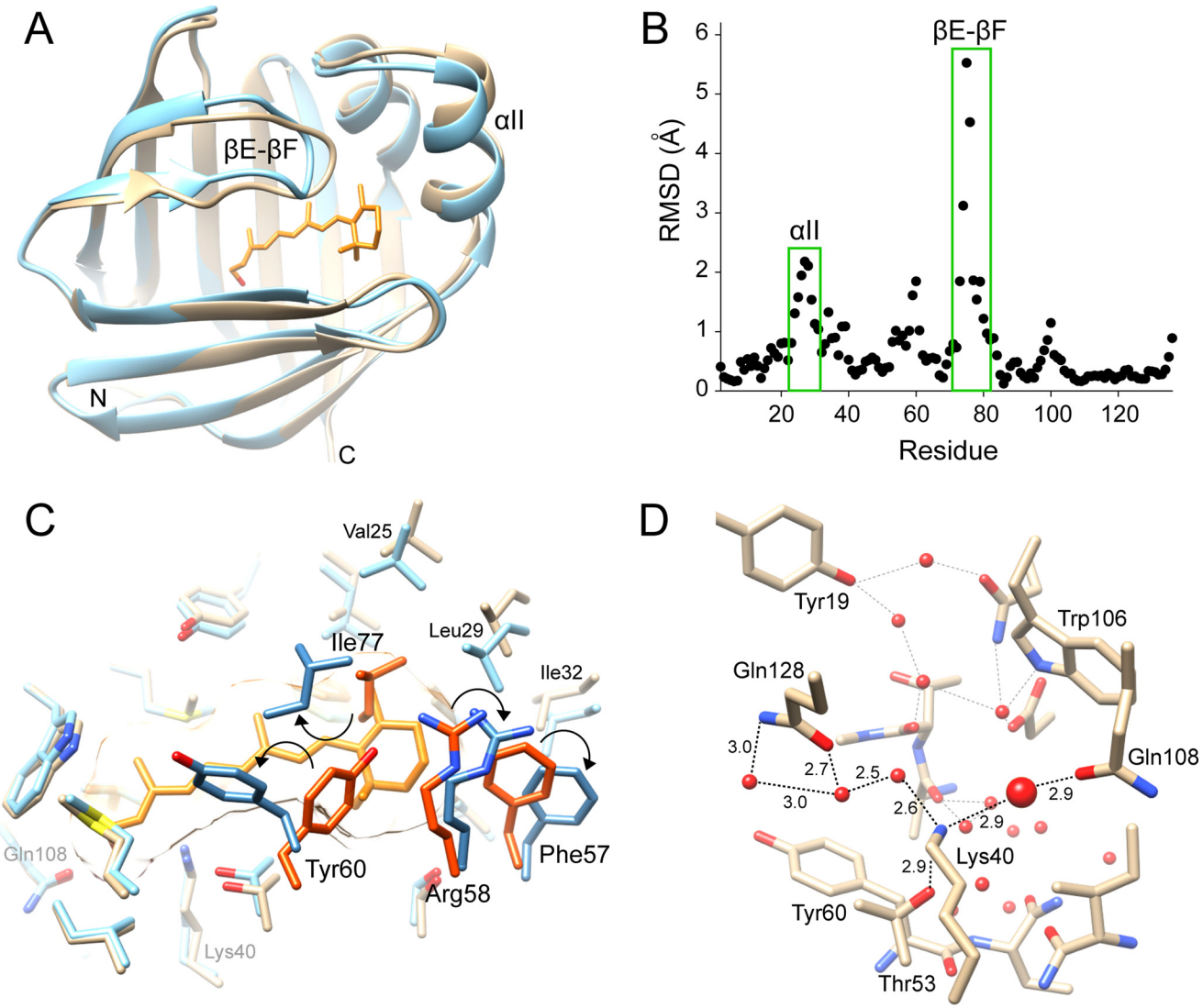

FIGURE 5. **Overview of the structure of apo-hCRBP1 and its comparison with the holo-form.** *A*, *ribbon representation* of superimposed structures of the all-*trans*-retinol holo- (PDB code 5HBS) and apoprotein (PDB code 5H9A) *colored* in *light blue* and *orange*, respectively. Hairpin turns between β-strands βE-βF and α-helix II reveal the highest level of conformational alterations. *B*, α-carbon root mean square deviations calculated between apo- and all-*trans*-retinol holoprotein as a function of residue position. Root mean square deviations (*RMSD*) for amino acids that belong to the βE-βF turn and α-helix II are indicated. *C*, differences in conformation of the side chains in hCRBP1 induced by ligand binding (holoprotein, *light blue*; apo-form, *light orange*). Residues that show the most significant changes are *labeled*. The side chains of Phe-57, Arg-58, Tyr-60, and Ile-77 that contribute to steric hindrance in the apoprotein are *labeled* with *darker colors*. Their shifts in position are marked by *arrows*. *D*, hydrogen bond network in apo-hCRBP1. All waters are represented by *red spheres*. The water molecule that is located at the position of a hydroxyl group of all-*trans*-retinol in holo-protein is shown with a *larger diameter*.

Discussion

The mechanistic basis for retinoid interactions with CRBPs has been the subject of extensive studies that have not yet converged into a general model for ligand binding or release. The major difficulty in formulating such a model was due to the relatively stable conformation of the apo-forms of CRBP2, -3, and -4, which are virtually identical except for the side chains of certain amino acids (10, 11, 32, 55). Thus, these data did not provide obvious evidence for the dynamic portal entrance leading to the binding cavity. However, the solution structures of rCRBP1 and CRBP2 determined by multidimensional NMR spectroscopy drew a different picture, revealing high local flexibility of the polypeptide main chain that predominantly affected the βE-βF turn and, to a lesser degree, the βC-βD loop (37, 58). This observation was further confirmed by mass spectrometry methods indicating that a localized backbone disorder resulted in increased rates of hydrogen/deuterium exchange in these regions of rCRBP1 (59).

In contrast to previous crystallographic data, the high resolution x-ray structures of hCRBP1 reported herein revealed an unanticipated conformational transformation in response to ligand binding, which affected the side and main chains that frame the ligand entry portal. Surprisingly, comparison of the apo- and holo-structures indicated that the dominant orientations of the side chains spatially close to the internal cavity blocked access to this site by narrowing the aperture of the entrance. This scenario strongly suggests a pivotal role for local structural dynamics in providing retinoid access to the binding site and fosters a tempting speculation about the putative

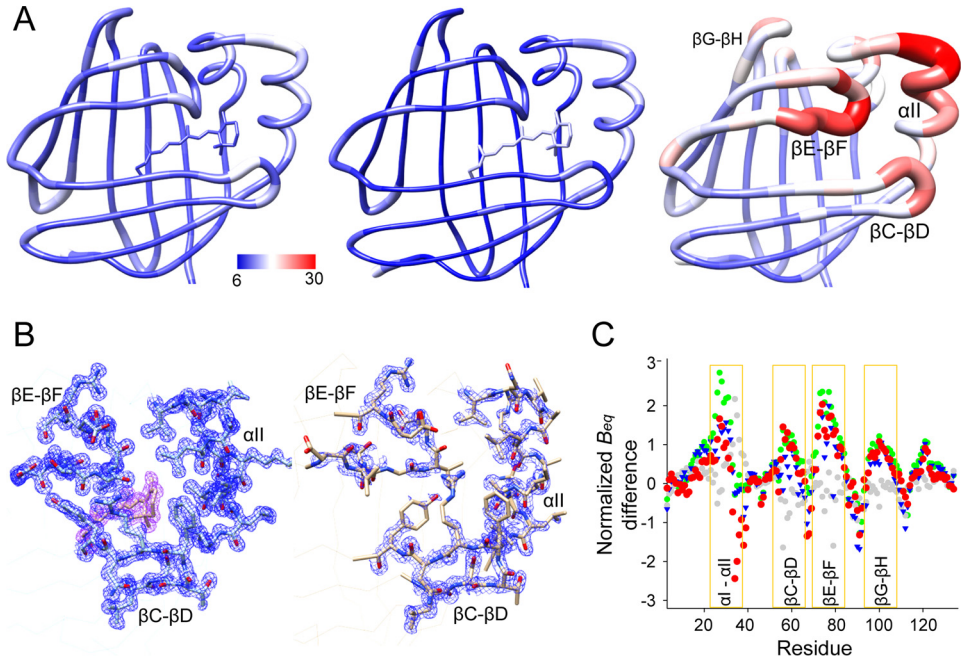

FIGURE 6. **Differences in the equivalent isotropic *B*-factors between apo- and holo-hCRBP1.** *A*, *graphic representation* of the residue average B_{eq} in all-*trans*-retinol holoprotein (*left*, PDB code 5HBS), its retinylamine-bound state (*middle*, PDB code 5HA1), and apo-form (*right*, PDB code 5H9A) *colored* from low to high (*blue* to *red*). Regions of the apo-hCRBP1 with the highest conformational flexibility are identified by *labels*. *B*, $2F_o - F_c$ electron density maps (*blue mesh*) of α-helix II and hairpin turns βC-βD and βE-βF for a 1.21 Å structure of all-*trans*-retinol holo-hCRBP1 (*left*) (PDB code 5H8T) and apoprotein (*right*). The *purple mesh* represents electron density for the ligand. All maps were contoured at 1.2σ. *C*, comparison of the normalized B_{eq}. The plot represents relative differences and indicates regions with increased conformational dynamics. The *color scheme* corresponds to the following paired structures: *green*, apo- (PDB code 5H9A) *versus* vitamin A holo- (0.89 Å resolution structure, PDB code 5HBS); *blue*, apo- (PDB code 5H9A) *versus* vitamin A holo- (1.21 Å, PDB code 5H8T); *red*, apo- (PDB code 5H9A) *versus* retinylamine holo- (PDB code 5HA1); and *gray*, vitamin A holo- (PDB code 5H8T) *versus* retinylamine holo-hCRBP1 (PDB code 5HA1).

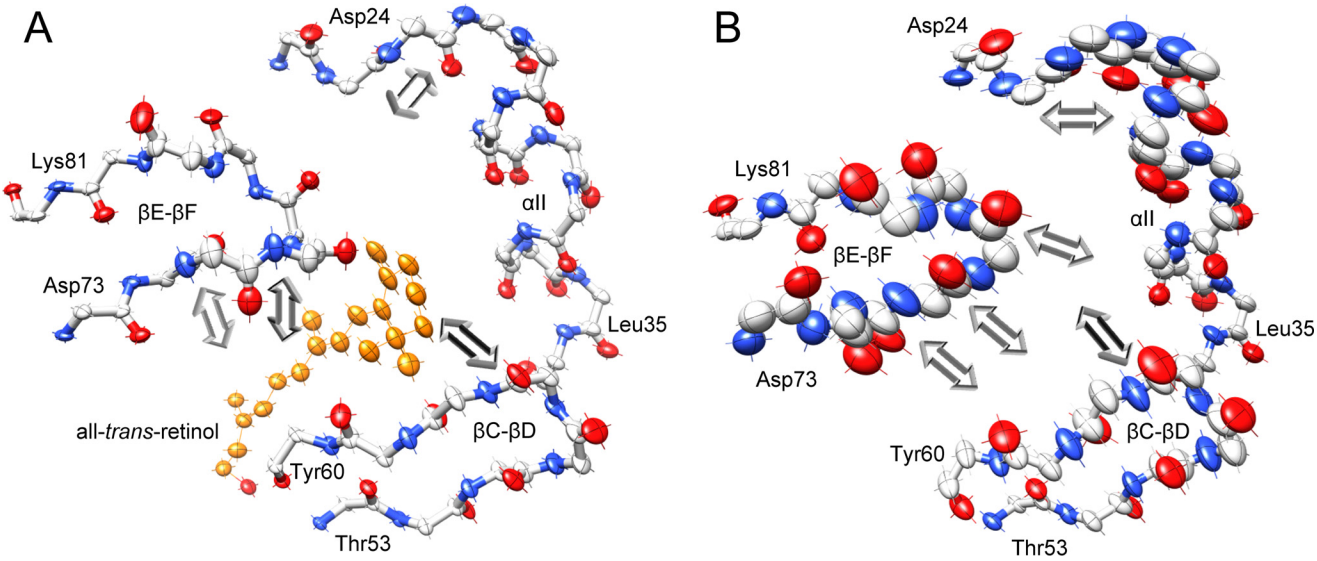

FIGURE 7. **Changes in the directional mobility of the portal region upon the ligand binding.** Individual atom anisotropic thermal ellipsoids are shown at the 25% probability level for the backbone atoms of all-*trans*-retinol-bound hCRBP1, PDB code 5H8T (*A*), and its apo-form, PDB code 5H9A (*B*). The orientations of the major vibrational axis for selected atoms in the βE-βF loop are *marked* with *arrows*. The *length* of *arrows* is arbitrarily exaggerated for clarity. *Red*, oxygen; *blue*, nitrogen; *gray*, carbon. Vitamin A molecule is *colored orange*.

mechanism for ligand recognition. How then can retinoids find their way to the binding cavity? *In vivo*, the interaction of vitamin A with CRBP1 occurs in the vicinity of lipid membranes. However, experiments done *in vitro* clearly indicate that the apoprotein binds all-*trans*-retinol spontaneously without the assistance of specific microenvironments, lipid membranes, or other proteins. Thus, it seems plausible that the initial interaction of the retinoid polyene chain with the mobile portal region could shift the equilibrium toward the latter's more open conformation and allow the ligand to slip deeper into the binding cavity. Once inside, hydrophobic interactions with the ligand's β-ionone ring could stabilize the conformation of the protein's βC-βD and βE-βF turns as well as α-helix II, locking vitamin A inside. These interactions appear to be critical for discrimination between retinoids and other hydrophobic ligands and thus could provide binding specificity.

Interestingly, similar conformational changes were observed in zebrafish CRBP, an ortholog of mammalian CRBP2 (56). Although the exact positions of the side chain atoms of Phe-57, Arg-58, Tyr-60, and Ile-77 (Leu-77 in zebrafish) differ from those found in apo-hCRBP1, they all occupy some of the space reserved for retinol in the holoprotein and thus had to be displaced upon ligand binding. This correlation could indicate a common evolutionarily conserved interaction mechanism with retinoids in the CRBP family.

More intriguing than binding is the question of targeted release of vitamin A from CRBP1. It is tempting to speculate that ligand liberation requires a transition back to the dynamic state of the portal region or its alternative conformation. Previous studies showed that spontaneous all-*trans*-retinol dissociation could be achieved at a relatively low pH (<4.0) or in a high concentration of alcohols (>20%) (60). Additionally, lipid membranes did not stimulate an effective release. If we consider that vitamin A needs to be transported from the plasma membrane or its storage sites to specific compartments within the cell, it becomes clear that this cannot be a stochastic process. Thus, targeted release of retinoids could be facilitated instead by specific interactions of CRBP1 with its protein binding partners, which are still unknown.

High resolution structures of hCRBP1 allowed us to map hydrogen bond networks in the binding site and investigate their role in ligand affinity. The higher affinity for all-*trans*-retinol in CRBP1 and -2 can be attributed to the formation of a hydrogen bond between the retinol hydroxyl group and ϵ^1-carbonyl oxygen of Gln-108. The significance of this residue is underscored by the fact that its substitution to histidine in CRBP3 and -4 lowered ligand affinity by a factor of 10 (10, 11). By analyzing the structure of hCRBP1, we provide convincing evidence that the canonical interaction of all-*trans*-retinol with Gln-108 is supplemented by an additional hydrogen bond formed with the amino group of Lys-40 (Fig. 3*B*). The Lys-40 interaction clearly contributes to the binding, as illustrated by the retinylamine example. The impossibility for hydrogen bonding with Lys-40 increased K_d values for retinylamine to 64.1 nM from the 18.6 nM determined for all-*trans*-retinol under identical experimental conditions (Fig. 4*B*). Importantly, the affinity measured for retinylamine corresponds closely to that calculated for all-*trans*-retinal (K_d = 50 nM) (61). Because of the potentially free rotation of the Gln-108 side chain in hCRBP1, the retinal carbonyl could form a hydrogen bond with its ϵ^2-amine group. However, similar to retinylamine, the retinal carbonyl cannot interact with Lys-40. The above finding provided additional evidence for the role of Lys-40 in hCRBP1 that ensures the highest affinity for vitamin A among CRBPs. To shed more light on the interaction of retinoids inside the binding pocket, we attempted to crystalize hCRBP1 in complex with all-*trans*-retinal. Unfortunately, the protein crystals obtained revealed a very low occupancy for this ligand. Thus, it might be that the efficiency of all-*trans*-retinal binding is limited by a residual network of water molecules in the apoprotein that mediated hydrogen bonds between Gln-108 and Lys-40, thereby limiting the ability of the Gln-108 side chain to rotate favorably for aldehyde binding.

In conclusion, crystal structures of hCRBP1 offer valuable new insights into the structure-function relationships of the retinol-binding protein family. The outcome of this study explains the importance of the entry portal region and its involvement in conformational changes associated with ligand binding and provides an alternative view of the interactions of the retinoid moiety in the hCRBP1 binding site. Importantly, our data clarify some of the controversies that have arisen about different findings obtained with crystal and in-solution structures of CRBPs.

Author Contributions—M. G. conceived and designed the study. J. A. S., J. M. A., S. C., P. D. K., S. B., and M. G. performed experiments and analyzed the data. M. G. wrote the manuscript with valuable input from J. A. S. and J. M. A. All authors reviewed the results as well as edited and approved the final version of the manuscript.

Acknowledgments—We thank L. T. Webster, Jr. for help in editing the manuscript. This work is based upon research conducted at the Northeastern Collaborative Access Team beamlines, which are funded by NIGMS, National Institutes of Health (NIH), Grant P41 GM103403. The Pilatus 6M detector on the 24-ID-C beamline is funded by NIH-ORIP HEI Grant S10 RR029205. This research used resources of the Advanced Photon Source, a United States Department of Energy (DOE) Office of Science User Facility operated for the DOE Office of Science by Argonne National Laboratory under Contract DE-AC02-06CH11357. We also thank the staff of the SLAC National Accelerator Laboratory (Menlo Park, CA), operated by Stanford University for the DOE Office of Science. Use of the Stanford Synchrotron Radiation Lightsource, SLAC National Accelerator Laboratory, is supported by the DOE Office of Science, Office of Basic Energy Sciences, under Contract DE-AC02-76SF00515. The SSRL Structural Molecular Biology Program is supported by the DOE Office of Biological and Environmental Research and by NIGMS, NIH, Grant P41GM103393.

References

1. Álvarez, R., Vaz, B., Gronemeyer, H., and de Lera, Á. R. (2014) Functions, therapeutic applications, and synthesis of retinoids and carotenoids. *Chem. Rev.* **114,** 1–125
2. Blomhoff, R., and Blomhoff, H. K. (2006) Overview of retinoid metabolism and function. *J. Neurobiol.* **66,** 606–630
3. O'Byrne, S. M., and Blaner, W. S. (2013) Retinol and retinyl esters: biochemistry and physiology. *J. Lipid Res.* **54,** 1731–1743
4. Al Tanoury, Z., Piskunov, A., and Rochette-Egly, C. (2013) Vitamin A and retinoid signaling: genomic and nongenomic effects. *J. Lipid Res.* **54,** 1761–1775
5. Noy, N. (2000) Retinoid-binding proteins: mediators of retinoid action. *Biochem. J.* **348,** 481–495
6. Kono, N., and Arai, H. (2015) Intracellular transport of fat-soluble vitamins A and E. *Traffic* **16,** 19–34
7. Chytil, F., and Ong, D. E. (1983) Cellular retinol-binding and retinoic acid-binding proteins. *Adv. Nutr. Res.* **5,** 13–29
8. Schaap, F. G., van der Vusse, G. J., and Glatz, J. F. (2002) Evolution of the family of intracellular lipid binding proteins in vertebrates. *Mol. Cell. Biochem.* **239,** 69–77
9. Bankaitis, V. A., Mousley, C. J., and Schaaf, G. (2010) The Sec14 superfamily and mechanisms for crosstalk between lipid metabolism and lipid signaling. *Trends Biochem. Sci.* **35,** 150–160
10. Folli, C., Calderone, V., Ottonello, S., Bolchi, A., Zanotti, G., Stoppini, M., and Berni, R. (2001) Identification, retinoid binding, and x-ray analysis of a human retinol-binding protein. *Proc. Natl. Acad. Sci. U.S.A.* **98,**

3710–3715
11. Folli, C., Calderone, V., Ramazzina, I., Zanotti, G., and Berni, R. (2002) Ligand binding and structural analysis of a human putative cellular retinol-binding protein. *J. Biol. Chem.* **277,** 41970–41977
12. Eriksson, U., Das, K., Busch, C., Nordlinder, H., Rask, L., Sundelin, J., Sällström, J., and Peterson, P. A. (1984) Cellular retinol-binding protein. Quantitation and distribution. *J. Biol. Chem.* **259,** 13464–13470
13. Kato, M., Kato, K., and Goodman, D. S. (1984) Immunocytochemical studies on the localization of plasma and of cellular retinol-binding proteins and of transthyretin (prealbumin) in rat liver and kidney. *J. Cell Biol.* **98,** 1696–1704
14. Saari, J. C., Bunt-Milam, A. H., Bredberg, D. L., and Garwin, G. G. (1984) Properties and immunocytochemical localization of 3 retinoid-binding proteins from bovine retina. *Vision Res.* **24,** 1595–1603
15. Li, E., Demmer, L. A., Sweetser, D. A., Ong, D. E., and Gordon, J. I. (1986) Rat cellular retinol-binding protein-Ii: use of a cloned cDNA to define its primary structure, tissue-specific expression, and developmental regulation. *Proc. Natl. Acad. Sci. U.S.A.* **83,** 5779–5783
16. Vogel, S., Mendelsohn, C. L., Mertz, J. R., Piantedosi, R., Waldburger, C., Gottesman, M. E., and Blaner, W. S. (2001) Characterization of a new member of the fatty acid-binding protein family that binds all-*trans*-retinol. *J. Biol. Chem.* **276,** 1353–1360
17. MacDonald, P. N., and Ong, D. E. (1987) Binding specificities of cellular retinol-binding protein and cellular retinol-binding protein, type II. *J. Biol. Chem.* **262,** 10550–10556
18. Levin, M. S., Locke, B., Yang, N. C., Li, E., and Gordon, J. I. (1988) Comparison of the ligand binding properties of two homologous rat apocellular retinol-binding proteins expressed in *Escherichia coli*. *J. Biol. Chem.* **263,** 17715–17723
19. Kawaguchi, R., Yu, J., Ter-Stepanian, M., Zhong, M., Cheng, G., Yuan, Q., Jin, M., Travis, G. H., Ong, D., and Sun, H. (2011) Receptor-mediated cellular uptake mechanism that couples to intracellular storage. *ACS Chem. Biol.* **6,** 1041–1051
20. Kawaguchi, R., Yu, J., Honda, J., Hu, J., Whitelegge, J., Ping, P., Wiita, P., Bok, D., and Sun, H. (2007) A membrane receptor for retinol binding protein mediates cellular uptake of vitamin A. *Science* **315,** 820–825
21. Herr, F. M., and Ong, D. E. (1992) Differential interaction of lecithin-retinol acyltransferase with cellular retinol binding proteins. *Biochemistry* **31,** 6748–6755
22. Ghyselinck, N. B., Båvik, C., Sapin, V., Mark, M., Bonnier, D., Hindelang, C., Dierich, A., Nilsson, C. B., Håkansson, H., Sauvant, P., Azaïs-Braesco, V., Frasson, M., Picaud, S., and Chambon, P. (1999) Cellular retinol-binding protein I is essential for vitamin A homeostasis. *EMBO J.* **18,** 4903–4914
23. Saari, J. C., Nawrot, M., Garwin, G. G., Kennedy, M. J., Hurley, J. B., Ghyselinck, N. B., and Chambon, P. (2002) Analysis of the visual cycle in cellular retinol-binding protein type I (CRBPI) knockout mice. *Invest. Ophthalmol. Vis. Sci.* **43,** 1730–1735
24. Golczak, M., Kuksa, V., Maeda, T., Moise, A. R., and Palczewski, K. (2005) Positively charged retinoids are potent and selective inhibitors of the trans-cis isomerization in the retinoid (visual) cycle. *Proc. Natl. Acad. Sci. U.S.A.* **102,** 8162–8167
25. Maeda, A., Maeda, T., Golczak, M., and Palczewski, K. (2008) Retinopathy in mice induced by disrupted all-trans-retinal clearance. *J. Biol. Chem.* **283,** 26684–26693
26. Zhang, J., Dong, Z., Mundla, S. R., Hu, X. E., Seibel, W., Papoian, R., Palczewski, K., and Golczak, M. (2015) Expansion of first-in-class drug candidates that sequester toxic all-trans-retinal and prevent light-induced retinal degeneration. *Mol. Pharmacol.* **87,** 477–491
27. Golczak, M., Imanishi, Y., Kuksa, V., Maeda, T., Kubota, R., and Palczewski, K. (2005) Lecithin:retinol acyltransferase is responsible for amidation of retinylamine, a potent inhibitor of the retinoid cycle. *J. Biol. Chem.* **280,** 42263–42273
28. Golczak, M., Sears, A. E., Kiser, P. D., and Palczewski, K. (2015) LRAT-specific domain facilitates vitamin A metabolism by domain swapping in HRASLS3. *Nat. Chem. Biol.* **11,** 26–32
29. Maeda, A., Maeda, T., Golczak, M., Imanishi, Y., Leahy, P., Kubota, R., and Palczewski, K. (2006) Effects of potent inhibitors of the retinoid cycle on visual function and photoreceptor protection from light damage in mice. *Mol. Pharmacol.* **70,** 1220–1229
30. Sacchettini, J. C., Gordon, J. I., and Banaszak, L. J. (1989) Crystal structure of rat intestinal fatty-acid-binding protein. Refinement and analysis of the *Escherichia coli*-derived protein with bound palmitate. *J. Mol. Biol.* **208,** 327–339
31. Sacchettini, J. C., Gordon, J. I., and Banaszak, L. J. (1989) Refined apoprotein structure of rat intestinal fatty acid binding protein produced in *Escherichia coli*. *Proc. Natl. Acad. Sci. U.S.A.* **86,** 7736–7740
32. Winter, N. S., Bratt, J. M., and Banaszak, L. J. (1993) Crystal structures of holo- and apo-cellular retinol-binding protein II. *J. Mol. Biol.* **230,** 1247–1259
33. Cowan, S. W., Newcomer, M. E., and Jones, T. A. (1993) Crystallographic studies on a family of cellular lipophilic transport proteins: refinement of P2 myelin protein and the structure determination and refinement of cellular retinol-binding protein in complex with all-*trans*-retinol. *J. Mol. Biol.* **230,** 1225–1246
34. Nossoni, Z., Assar, Z., Yapici, I., Nosrati, M., Wang, W., Berbasova, T., Vasileiou, C., Borhan, B., and Geiger, J. (2014) Structures of holo wild-type human cellular retinol-binding protein II (hCRBPII) bound to retinol and retinal. *Acta Crystallogr. D Biol. Crystallogr.* **70,** 3226–3232
35. Hodsdon, M. E., and Cistola, D. P. (1997) Ligand binding alters the backbone mobility of intestinal fatty acid-binding protein as monitored by ^{15}N NMR relaxation and ^{1}H exchange. *Biochemistry* **36,** 2278–2290
36. Lu, J., Lin, C. L., Tang, C., Ponder, J. W., Kao, J. L., Cistola, D. P., and Li, E. (1999) The structure and dynamics of rat apo-cellular retinol-binding protein II in solution: comparison with the x-ray structure. *J. Mol. Biol.* **286,** 1179–1195
37. Franzoni, L., Lücke, C., Pérez, C., Cavazzini, D., Rademacher, M., Ludwig, C., Spisni, A., Rossi, G. L., and Rüterjans, H. (2002) Structure and backbone dynamics of apo- and holo-cellular retinol-binding protein in solution. *J. Biol. Chem.* **277,** 21983–21997
38. Xiao, H., and Kaltashov, I. A. (2005) Transient structural disorder as a facilitator of protein-ligand binding: native H/D exchange-mass spectrometry study of cellular retinoic acid binding protein I. *J. Am. Soc. Mass. Spectrom.* **16,** 869–879
39. Burger, A., Berendes, R., Voges, D., Huber, R., and Demange, P. (1993) A rapid and efficient purification method for recombinant annexin V for biophysical studies. *FEBS Lett.* **329,** 25–28
40. Bridges, C. D. (1975) Storage, distribution and utilization of vitamins A in the eyes of adult amphibians and their tadpoles. *Vision Res.* **15,** 1311–1323
41. Lakowicz, J. R. (1999) *Principles of Fluorescence Spectroscopy*, 2nd Ed., pp. 53–56, Kluwer Academic/Plenum, New York
42. Ong, D. E., and Chytil, F. (1978) Cellular retinol-binding protein from rat liver: purification and characterization. *J. Biol. Chem.* **253,** 828–832
43. Leslie, A. G. W., and Powell, H. R. (2007) Processing diffraction data with MOSFLM. *NATO Sci. Ser. II* **245,** 41–51
44. Kabsch, W. (2010) Integration, scaling, space-group assignment and post-refinement. *Acta Crystallogr. D Biol. Crystallogr.* **66,** 133–144
45. Winn, M. D., Ballard, C. C., Cowtan, K. D., Dodson, E. J., Emsley, P., Evans, P. R., Keegan, R. M., Krissinel, E. B., Leslie, A. G. W., McCoy, A., McNicholas, S. J., Murshudov, G. N., Pannu, N. S., Potterton, E. A., Powell, H. R., *et al.* (2011) Overview of the CCP4 suite and current developments. *Acta Crystallogr. D Biol. Crystallogr.* **67,** 235–242
46. Emsley, P., and Cowtan, K. (2004) Coot: model-building tools for molecular graphics. *Acta. Crystallogr. D Biol. Crystallogr.* **60,** 2126–2132
47. Collaborative Computational Project, Number 4 (1994) The CCP4 Suite: Programs for Protein Crystallography. *Acta Crystallogr. D Biol. Crystallogr.* **50,** 760–763
48. Adams, P. D., Afonine, P. V., Bunkóczi, G., Chen, V. B., Davis, I. W., Echols, N., Headd, J. J., Hung, L. W., Kapral, G. J., Grosse-Kunstleve, R. W., McCoy, A. J., Moriarty, N. W., Oeffner, R., Read, R. J., Richardson, D. C., Richardson, J. S., Terwilliger, T. C., and Zwart, P. H. (2010) PHENIX: a comprehensive Python-based system for macromolecular structure solution. *Acta Crystallogr. D Biol. Crystallogr.* **66,** 213–221
49. Chen, V. B., Arendall, W. B., 3rd, Headd, J. J., Keedy, D. A., Immormino, R. M., Kapral, G. J., Murray, L. W., Richardson, J. S., and Richardson, D. C. (2010) MolProbity: all-atom structure validation for macromolecular

crystallography. *Acta Crystallogr. D Biol. Crystallogr.* **66,** 12–21
50. Pettersen, E. F., Goddard, T. D., Huang, C. C., Couch, G. S., Greenblatt, D. M., Meng, E. C., and Ferrin, T. E. (2004) UCSF Chimera: a visualization system for exploratory research and analysis. *J. Comput. Chem.* **25,** 1605–1612
51. Schneider, B., Gelly, J. C., de Brevern, A. G., and Černý, J. (2014) Local dynamics of proteins and DNA evaluated from crystallographic B factors. *Acta Crystallogr. D Biol. Crystallogr.* **70,** 2413–2419
52. Trueblood, K. N., Burgi, H. B., Burzlaff, H., Dunitz, J. D., Gramaccioli, C. M., Schulz, H. H., Shmueli, U., and Abrahams, S. C. (1996) Atomic displacement parameter nomenclature: report of a subcommittee on atomic displacement parameter nomenclature. *Acta. Crystallogr. A* **52,** 770–781
53. Merritt, E. A. (1999) Comparing anisotropic displacement parameters in protein structures. *Acta Crystallogr. D Biol. Crystallogr.* **55,** 1997–2004
54. Newcomer, M. E., Liljas, A., Eriksson, U., Sundelin, J., Rask, L., and Peterson, P. A. (1981) Crystallization of and preliminary x-ray data for an intracellular vitamin A-binding protein from rat liver. *J. Biol. Chem.* **256,** 8162–8163
55. Tarter, M., Capaldi, S., Carrizo, M. E., Ambrosi, E., Perduca, M., and Monaco, H. L. (2008) Crystal structure of human cellular retinol-binding protein II to 1.2 A resolution. *Proteins* **70,** 1626–1630
56. Calderone, V., Folli, C., Marchesani, A., Berni, R., and Zanotti, G. (2002) Identification and structural analysis of a zebrafish apo and holo cellular retinol-binding protein. *J. Mol. Biol.* **321,** 527–535
57. Rosenfield, R. E., Trueblood, K. N., and Dunitz, J. D. (1978) Test for rigid-body vibrations, based on a generalization of hirshfeld rigid-bond postulate. *Acta Crystallogr. A* **34,** 828–829
58. Lu, J., Cistola, D. P., and Li, E. (2003) Two homologous rat cellular retinol-binding proteins differ in local conformational flexibility. *J. Mol. Biol.* **330,** 799–812
59. Careri, M., Elviri, L., Mangia, A., Zagnoni, I., Torta, F., Cavazzini, D., and Rossi, G. L. (2006) Mass spectrometry techniques for detection of ligand-dependent changes in the conformational flexibility of cellular retinol-binding protein type I localized by hydrogen/deuterium exchange. *Rapid Commun. Mass Spectrom.* **20,** 1973–1980
60. Torta, F., Dyuysekina, A. E., Cavazzini, D., Fantuzzi, A., Bychkova, V. E., and Rossi, G. L. (2004) Solvent-induced ligand dissociation and conformational states of cellular retinol-binding protein type I. *Biochim. Biophys. Acta* **1703,** 21–29
61. Li, E., Qian, S. J., Yang, N. C., d'Avignon, A., and Gordon, J. I. (1990) 19F nuclear magnetic resonance studies of 6-fluorotryptophan-substituted rat cellular retinol binding protein II produced in *Escherichia coli*: an analysis of four tryptophan substitution mutants and their interactions with all-*trans*-retinol. *J. Biol. Chem.* **265,** 11549–11554